Mechanism of charge transport in ITO/$[GeO_x]_{(z)}[SiO_2]_{(1-z)}/n^+$-Si MIS structures

© I.D. Yushkov[1,2], A.A. Gismatulin[1], G.N. Kamaev[1], M. Vergnat[3], V.A. Volodin[1,2]

[1] Rzhanov Institute of Semiconductor Physics, Siberian Branch, Russian Academy of Sciences,
630090 Novosibirsk, Russia
[2] Novosibirsk State University,
630090 Novosibirsk, Russia
[3] Université de Lorraine,
F-54000 Nancy, France

E-mail: ivanjushkov@gmail.com

Received July 17, 2025
Revised August 12, 2025
Accepted August 14, 2025

The mechanism of charge transport in metal-insulator-semiconductor (MIS) ITO/$[GeO_x]_{(z)}[SiO_2]_{(1-z)}$ $(0.25 \leq z \leq 1)/n^+$-Si structures with germanosilicate glass films fabricated by electron beam evaporation of germanium oxide and silicon oxide powders in vacuum are studied. The ITO top contact was deposited on the surface of the dielectric layer by magnetron sputtering. By IR spectroscopy, Ge−O, Si−O and Ge−O−Si bonds are observed in the films $[GeO_x]_{(z)}[SiO_2]_{(1-z)}$ $(0.25 \leq z \leq 0.75)$. The experimental current-voltage characteristics measured at different temperatures are approximated using both contact-limited and bulk-limited models of charge transport in the dielectric. It is shown that the conduction mechanism is most adequately described by the model of space charge space-limited current. The parameters of traps in the dielectric are determined within this model.

Keywords: MIS structure, Charge transport, Infrared spectroscopy.

DOI: 10.61011/SC.2025.06.62060.8396

1. Introduction

The development of digital technologies, such as storing and processing large amounts of data, requires improving the characteristics of memory devices: increasing the amount of memory, increasing the speed of rewriting, increasing the number of rewriting cycles, and reducing power consumption during rewriting operations. Modern types of memory, such as flash memory, have already reached their technological limit. In this regard, the creation of a new universal non-volatile memory is an important and urgent problem of modern nanoelectronics. Resistive random-access memory (ReRAM) technology is actively developing and becoming more popular due to its advantages over other types of memory, such as high energy efficiency, high rewriting speed and high endurance. The ReRAM technology is based on materials with multiple resistive states that can persist when disconnected from the power supply [1,2]. It is worth noting that ReRAM memory matrices have been embedded in cache memory chips manufactured by Fujitsu, Panasonic, and others for almost ten years [3].

Previously, our group conducted studies of metal-dielectric-semiconductor (MDS) structures based on germanosilicate glasses, where several stable resistive states were found [4,5]. The main advantage of germanosilicate glasses is the possibility of modulating trap parameters, for example, it is possible to form deep traps (germanium clusters) by annealing [6]. It is also possible to change the composition of the films, the amount of germanium, silicon and oxygen. An interesting property of the material $[GeO_x]_{(z)}[SiO_2]_{(1-z)}$ is the possibility of combining the stability of resistive switching characteristics (as in SiO_x) and switching energy efficiency, since GeO_x has a low binding enthalpy Ge−O [4,7,8].

To optimize the properties of memristors based on $[GeO_x]_{(z)}[SiO_2]_{(1-z)}$ films and obtain more stable resistive switching cycles, it is important to know the parameters of traps in dielectric films that determine charge transport. Previously, we studied the mechanisms of conduction in films of similar composition, but grown on a p^+-silicon substrate: the volt-ampere characteristics (VAC) were analyzed with forward displacement, i.e. with the injection of holes from a silicon substrate [9]. We studied in this paper the mechanisms of charge transport in MDS structures based on germanosilicate glasses $[GeO_x]_{(z)}[SiO_2]_{(1-z)}$ of various stoichiometry grown on a silicon n^+-substrate. For this purpose, the VAC (also with direct bias, i.e. with electron injection from a silicon substrate) was analyzed at various temperatures with an approximation of the experimental VAC calculated within the framework of the eight most common charge transfer models, which are described in more detail in Ref. [10].

2. Description of the experiment

2.1. Production of films and MDS structures

Films of nonstoichiometric germanosilicate glasses were obtained by high-vacuum electron beam evaporation and electron beam physical vapor deposition (EB-PVD). The

working chamber was pre-pumped to the residual pressure $10^{-9}-10^{-8}$ Torr. The films were deposited at room temperature, and during evaporation of the targets (germanium oxide and silicon oxide powders), the pressure in the chamber increased by 1–2 orders of magnitude. The films were deposited on n^+-Si(100) substrates (resistivity $\rho = 0.003 \pm 0.01$ ohms · cm) for electrophysical measurements and n-Si (100) ($\rho = 5.5 \pm 1$ Ohms · cm) for optical measurements. The natural oxide on the silicon substrate was etched with hydrofluoric acid. However, before being placed in a vacuum chamber, the substrates were exposed to an air atmosphere for several hours, respectively, they were coated with a thin layer of natural silicon oxide. The composition of the films was changed by varying the power ratio of the electron beams vaporizing the targets GeO_2 and SiO_2. As a result, $[GeO_x]_{(z)}[SiO_2]_{(1-z)}$ films of four compositions were obtained: $z = 1$, 0.75, 0.5, and 0.25; these samples are further designated as 1–4, respectively. It is important to note that, as it was established earlier in Refs. [11,12], when the target GeO_2 evaporates under such conditions, a film similar in composition to germanium monoxide — GeO_x is deposited, where x is 1.1–1.2.

Structural studies were carried out on initially deposited films, and for electrophysical studies, MD structures were formed: upper indium-tin oxide (ITO) contacts were deposited on the films by magnetron sputtering through a metal mask. The thickness of the contact pads was 150–200 nm, surface resistance was 40–60 Ohms/square, square area of the contact pad was 0.7×0.7 mm.

2.2. Film structure studies

The thickness and refractive and absorption indices were determined from experimental spectral ellipsometry data. The measurements were carried out using spectral ellipsometer „ELLIPS-1891-SAG“ (ISP SB RAS) with an optical range of 250–800 nm. Due to the difficulties of analyzing thin film thicknesses based on ellipsometry data in a situation where their optical constants are unknown, the refractive and absorption spectra were determined on satellite samples with an order of magnitude greater thickness, but obtained by the same method under the same conditions. Further, using the obtained optical parameters, the thicknesses of thin films were determined (Table 1).

Table 1. Thickness and optical parameters of samples 1–4

Sample	Thickness, nm	n	k
1	32	1.85	0.0116
2	20	1.74	0.0093
3	17	1.56	0.0051
4	18	1.50	0

Table 2. Sample composition 1–4

Sample	Ge, %	C, %	O, %	Si, %	Ge/Si	z
1	47.3	4.6	48.1	0.0	0.0	1
2	31.6	4.0	53.3	11.0	2.9	0.74
3	20.7	4.3	56.6	18.5	1.1	0.53
4	9.1	3.4	58.0	29.5	0.3	0.24

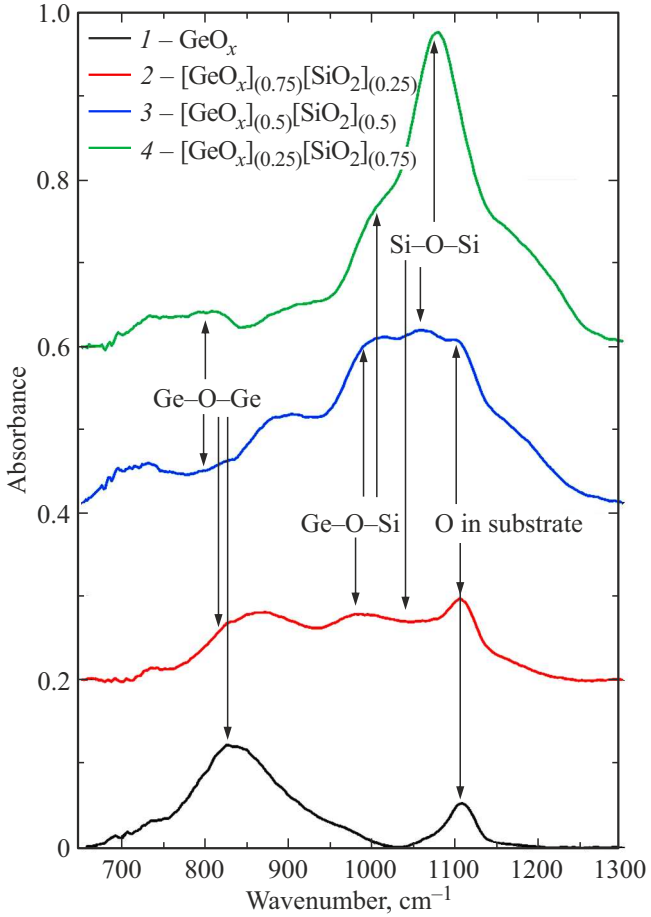

Figure 1. IR spectra of samples 1–4.

The energy spectrum and composition of $[GeO_x]_{(z)}[SiO_2]_{(1-z)}$ films were determined by analyzing X-ray photoelectron spectroscopy (XPS) data. The XPS spectra were recorded using SPECS photoelectron spectrometer (Germany) with a hemispherical analyzer PHOIBOS-150-MCD-9 (AlK_α-radiation, $h\nu = 1486.6$ eV, 150 W) with a transmission energy of 20 eV. XPS data were obtained for levels Ge $3d$, Si $2p$, C $1s$, O $1s$ and Ge $2p$. The composition and atomic ratio of the elements (Table 2) were calculated from the integral intensity of the photoelectron peaks (Ge $3d$, Si $2p$ and O $1s$) adjusted for theoretical data and sensitivity coefficients based on Scofield photoionization cross sections [13].

The infrared (IR) absorption spectra were recorded using an hboxFT-801 Fourier spectrometer manufactured by „SIMEX“, Novosibirsk, Russia. The spectral range of the device is 550–4000 cm^{-1}, the spectral resolution is set to 4 cm^{-1}. The spectrum of a n-type silicon substrate on which the films were grown was used as a reference signal. The measurements were carried out on satellite samples grown under exactly the same conditions, but the deposition

Table 3. Parameters calculated by the method of approximation of experimental VAC in the framework of various theoretical models

№	Effect Schottky	TAT	Effect Frenkel	The model Hill–Adachi	Model Makram–Ebeid and Lanno	Model Nasyrov–Gritsenko	Model Shklovsky–Efros
1	$m^* = 6 \cdot 10^{-9} m_e$ $W_0 = 0.32$ eV $\varepsilon_\infty = 1.8$	$m^* = 0.1 \cdot m_e$ $W_0 = 0.3$ eV $S = 5 \cdot 10^{-14}$ s^2	$N = 7 \cdot 10^7$ cm^{-3} $W = 0.4$ eV $\nu = 9.3 \cdot 10^{-3}$ s^{-1} $\varepsilon_\infty = 4.3$	$N = 6 \cdot 10^{19}$ cm^{-3} $W = 0.8$ eV $N = 7 \cdot 10^{-2}$ s^{-1} $\varepsilon_\infty = 1.7$	$N = 2 \cdot 10^8$ cm^{-3} $m^* = 0.2 m_e$ $W_t = 0.25$ eV $W_{opt} = 0.5$ eV $W_{ph} = 60$ MeV	$N = 5 \cdot 10^{18}$ cm^{-3} $m^* = 2.3 m_e$ $W_t = 0.1$ eV $W_{opt} = 0.4$ eV	$I_0 = 8.6 \cdot 10^{-5}$ A $W_e = 0.2$ eV $V_0 = 1.5$ eV $a = 0.6$ nm
2	$m^* = 2 \cdot 10^{-9} m_e$ $W_0 = 0.24$ eV $\varepsilon_\infty = 2.8$	$m^* = 0.32 \cdot m_e$ $W_0 = 0.2$ eV $S = 4 \cdot 10^{-14}$ m^2	$N = 4 \cdot 10^8$ cm^{-3} $W = 0.3$ eV $\nu = 7.3 \cdot 10^{-3}$ s^{-1} $\varepsilon_\infty = 11$	$N = 3 \cdot 10^{19}$ cm^{-3} $W = 1.1$ eV $N = 7 \cdot 10^{-3}$ s^{-1} $\varepsilon_\infty = 2.5$	$N = 5 \cdot 10^7$ cm^{-3} $m^* = 0.3 m_e$ $W_t = 0.25$ eV $W_{opt} = 0.5$ eV $W_{ph} = 60$ MeV $W_{ph} = 60$ MeV	$N = 6 \cdot 10^{19}$ cm^{-3} $m^* = 2.4 m_e$ $W_t = 0.4$ eV $W_{opt} = 0.8$ eV	$I_0 = 1.8 \cdot 10^{-4}$ A $W_e = 0.3$ eV $V_0 = 1.5$ eV $a = 1.5$ nm
3	$m^* = 10^{-7} m_e$ $W_0 = 0.12$ eV $\varepsilon_\infty = 10$	$m^* = 2.1 \cdot m_e$ $W_0 = 0.1$ eV $S = 4 \cdot 10^{-15}$ m^2	$N = 5 \cdot 10^{10}$ cm^{-3} $W = 0.2$ eV $N = 6 \cdot 10^{-3}$ s^{-1} $\varepsilon_\infty = 40$	$N = 3 \cdot 10^{20}$ cm^{-3} $W = 1.42$ eV $N = 5 \cdot 10^{-3}$ s^{-1} $\varepsilon_\infty = 3.7$	$N = 2 \cdot 10^{10}$ cm^{-3} $m^* = 4 m_e$ $W_t = 0.15$ eV $W_{opt} = 0.3$ eV $W_{ph} = 60$ MeV	$N = 6 \cdot 10^{20}$ cm^{-3} $m^* = 12 m_e$ $W_t = 0.15$ eV $W_{opt} = 0.75$ eV	$I_0 = 5.3 \cdot 10^{-3}$ A $W_e = 0.2$ eV $V_0 = 1.5$ eV $a = 0.5$ nm
4	$m^* = 2 \cdot 10^{-6} m_e$ $W_0 = 0.34$ eV $\varepsilon_\infty = 3.42$	$m^* = 0.46 \cdot m_e$ $W_0 = 0.3$ eV $S = 1 \cdot 10^{-12}$ m^2	$N = 5 \cdot 10^{11}$ cm^{-3} $W = 0.4$ eV $N = 1.3 \cdot 10^{-3}$ s^{-1} $\varepsilon_\infty = 14$	$N = 5 \cdot 10^{19}$ cm^{-3} $W = 1.1$ eV $N = 4.2$ s^{-1} $\varepsilon_\infty = 2.7$	$N = 10^{10}$ cm^{-3} $m^* = 4 m_e$ $W_t = 0.2$ eV $W_{opt} = 0.4$ eV $W_{ph} = 60$ MeV	$N = 6 \cdot 10^{19}$ cm^{-3} $m^* = 0.9 m_e$ $W_t = 0.33$ eV $W_{opt} = 1.62$ eV	$I_0 = 9 \cdot 10^{-2}$ A $W_e = 0.4$ eV $V_0 = 1.5$ eV $a = 1.2$ nm

Note. W_0 is the height of the triangular barrier, m^* is the effective electron mass, ε_∞ is the high frequency permittivity, N is the trap concentration, ν is the transition probability factor, W is the trap ionization energy, W_t is the thermal trap ionization energy, W_{opt} is the optical trap ionization energy, Wph is the phonon energy, V_0 is the amplitude of energy fluctuations, a is the spatial scale of potential fluctuations, W_e is the percolation energy.

time was longer, and the film thickness was ~ 300 nm. Also, these satellite samples were coated on top with a 20 nm thick protective layer SiO_2. Figure 1 shows the IR absorption spectra of all film compositions deposited on a *n*-Si substrate. An absorption peak is observed at 827 cm^{-1} in the spectrum of the sample 1 (GeO_x), corresponding to vibrations in the Ge–O bonds. This position corresponds to the GeO_x film of composition $x = 1.16$ [12,14].

Bands are observed in 2–4 films with the presence of silicon oxide corresponding to the absorption of vibrations of bonds of Si–O (≈ 1055 cm^{-1}) and Ge–O–Si (≈ 990 cm^{-1}), as well as the absorption band of Ge–O bonds (≈ 807 cm^{-1}). It is worth noting that the spectra also exhibit a small peak from absorption on the protective layer SiO_2 (≈ 1080 cm^{-1}) and a peak from absorption not fully compensated in the reference signal on oxygen fluctuations in the silicon substrate (1107 cm^{-1}).

It is known that nonstoichiometric germanosilicate glasses can contain clusters of amorphous germanium [4]. In this regard, it was decided to study the obtained thin films $[GeO_x]_{(z)}[SiO_2]_{(1-z)}$ for the presence of germanium clusters by Raman scattering (RS). The RS spectra were recorded using a Horiba Jobin Yvon T64000 spectrometer. A solid-state laser with $\lambda = 514.5$ nm was used as a source of excitation of RS spectra. The analysis of the obtained RS spectra did not show peaks corresponding to scattering by vibrations of Ge–Ge bonds, therefore, the RS spectra themselves are not given in the work.

2.3. Electrophysical studies

Electrophysical measurements of MDS structures based on $[GeO_x]_{(z)}[SiO_2]_{(1-z)}$ films were carried out in LTS420E stage manufactured by Linkam (UK) using Keythley 2400 electrometer and Linkam T95 temperature controller. The voltage scanning rate for the VAC was 0.05 V/s. Measurements were carried out at temperatures of 300, 325, 350 and 375 K.

To determine the mechanism of transport in MDS structures based on $[GeO_x]_{(z)}[SiO_2]_{(1-z)}$, experimental VAC recorded at various temperatures were compared with theoretical VAC calculated using the following theoretical models: Schottky effect [15,16], Thermally Assisted Tunneling (TAT) on contact [17–19], Frenkel effect [20,21], Hill-Adachi model [22,23], Shklovsky-Efros percolation model [24,25], multiphonon ionization model of Makram-Ebeid and Lanno traps [26], Nasyrov-Gritsenko phonon tunneling model [27] and a space-charge-limited current model (SCLC) [28–30]. The theoretical VAC was obtained by approximating the experimental VAC with the above models. The equations describing charge transfer and the model parameters are described in detail below.

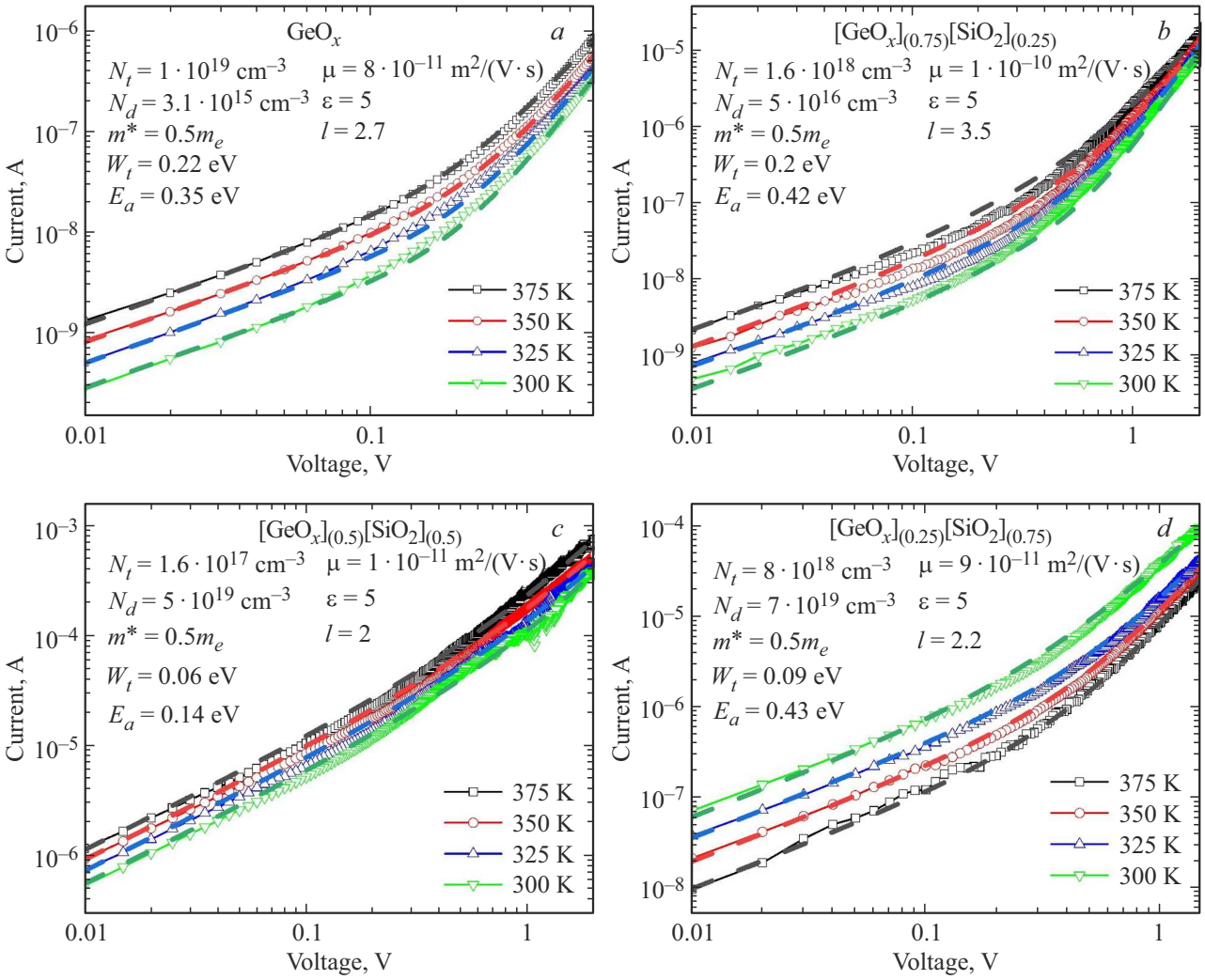

Figure 2. Experimental (line with empty dots) and theoretical (dotted line) VAC of samples 1 (*a*), 2 (*b*), 3 (*c*) and 4 (*d*).

3. Results and discussion

The parameters of the approximation of experimental VAC by all the above-mentioned models, except for the SCLC model, are presented in Table 3. The analysis of the data obtained allows us to conclude that within the framework of the considered models it is impossible to describe the VAC of the samples, since the values of the parameters obtained as a result of the VAC approximation do not correspond to the values obtained by other methods or have abnormally low or abnormally high values. Thus, for the Schottky effect, the resulting effective mass of an electron is abnormally low and is not comparable to the effective mass in SiO_2 or GeO_2 [31,32]. At the same time, the high-frequency dielectric constant ε_∞ obtained as a result of approximation does not correspond to the values calculated using the refractive index ($\varepsilon_\infty = n^2$). The resulting contact area in 10^5-10^7 in the TAT model is less than the actual contact area. For the Frenkel effect, the resulting trap concentration is abnormally small, since at this concentration the average distance between the traps exceeds the film thickness by 4–6 orders of magnitude. Similarly, the high-frequency dielectric constant ε_∞ significantly exceeds the values obtained from the refractive index. The high-frequency permittivity ε_∞ in the Hill-Adachi model also does not correspond to the values obtained by another method (ellipsometry). In addition, the theoretical value of the „transition probability coefficient“, ν, which is determined from the Einstein ratio $\nu = W/h$ (where W is the ionization energy of the trap, $h$is the Planck's constant), is underestimated and is equal to $\sim 10^{14}\,s^{-1}$. The Makram-Ebeid-Lanno and Nasyrov-Gritsenko models give overestimated values of effective masses. The applicability of the Shklovsky-Efros model is determined by the criterion of classical approximation, in which the electron does not tunnel through barriers. However, when using parameter a (spatial scale of fluctuations) as the width of the barrier, the probability of tunneling will be significant. As a result of the evaluation, the criterion of applicability of the Shklovsky-Efros model is not fulfilled.

Figure 2 shows the experimental VAC on a double logarithmic scale for all film compositions at different

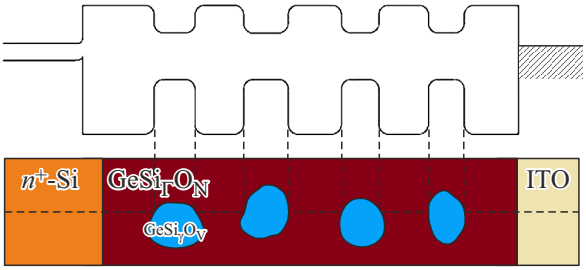

Figure 3. Zone diagram (top) and diagram (bottom) of MDS structures based on germanosilicate glasses.

temperatures and the theoretical VAC based on the SCLC model, as well as all the obtained parameters of the SCLC model.

A strong argument in favor of the SCLC model is that three sections are observed on all VCS: a linear section that describes scattering by defects in a dielectric, a quadratic section that describes the localization of free charge carriers on adhesion traps, and a section with a voltage degree > 2 that describes the exponential distribution of traps by energy. The expression for the VAC in the SCLC model looks like this [30,33,34]:

$$I = Se\mu n\frac{U}{d} + S\frac{9}{8}\mu\varepsilon\varepsilon_0\theta\frac{U^2}{d^3} + SN_c\mu e^{1-l}\left(\frac{\varepsilon\varepsilon_0 l}{N_c(l+1)}\right)^l\left(\frac{2l+1}{l+1}\right)^{l+1}\frac{U^{l+1}}{d^{2l+1}}, \quad (1)$$

$$n = \frac{2N_d}{1+\sqrt{1+\frac{4gN_d}{N_c}\exp\left(\frac{E_a}{k_BT}\right)}},$$

$$\theta = \frac{N_c}{N_t}\exp\left(-\frac{W_t}{k_BT}\right), \quad N_c = 2\left(\frac{2\pi m^* k_BT}{h^2}\right)^{3/2}, \quad (2)$$

where S is the contact area, e is the electron charge, μ is the electron mobility, n is the concentration of free carriers in the dielectric, U is the voltage, d is the dielectric thickness, ε is the static permittivity, ε_0 is the dielectric constant of vacuum, θ is the degree of trap filling, N_d is the concentration of donor-like defects, g is the degeneracy factor, N_c is the effective density of states, E_a is the activation energy of donor-like defects, k_B is the Boltzmann constant, T is the temperature, m^* is the effective mass of electrons, h is the Planck's constant, N_t is the trap concentration, W_t is the trap ionization energy and $l = T_t/T$, where T_t is a temperature parameter that characterizes the exponential the distribution of traps.

Thus, the SCLC model provides both the closest values of the VAC to the experimental ones and the most relevant parameters. For example, the concentration of traps in films is $10^{18}-10^{19}\,cm^{-3}$. In addition, the average distance between the traps is < 10 nm. The scale of potential fluctuations in SiO_x is also estimated at several nanometers [35]. It is assumed that such charge traps are fluctuations in composition in nonstoichiometric germanosilicate glasses.

Figure 3 shows a diagram of the energy range of the MDS structure without external displacement. The output of ITO is 4.62−4.81 eV [36]. Then, based on the difference in the yield of silicon and ITO, it can be assumed that a depleted layer with a bend in the energy bands of 0.5−0.7 eV is formed in the silicon substrate. The diagram in Figure 3 also shows nanoscale potential fluctuations (shown above) that occur due to composition fluctuations (shown below), similar to the non-stoichiometric TaO_x [37] and SiO_x [35].

4. Conclusion

Thus, the VAC of MDS structures based on $[GeO_x]_{(z)}[SiO_2]_{(1-z)}$ films as a dielectric $(0.25 \le z \le 1)$ has been analyzed. The experimental VAC measured at different temperatures are approximated using various models of charge transport in a dielectric. It is established that the conduction mechanism is most adequately described by the SCLC model, and the parameters of charge traps within this model are determined. Some differences in the parameters of the SCLC model obtained in this work with the parameters obtained earlier for structures on silicon substrates p^+-type [9] are probably related to the fact that films can have a bipolar type of conductivity. And in this particular case, electrons are injected, and holes in the case of silicon substrates of p^+-type [9]. It is necessary to produce special MDS structures with thicker films on weakly doped substrates to unambiguously establish the type of conductivity in $[GeO_x]_{(z)}[SiO_2]_{(1-z)}$ films, and this will be the subject of further studies. It should only be noted that the bipolar conductivity is observed in GeO_x films [38].

Funding

Regarding the study of structural and optical properties, the work was carried out within the framework of the state assignment (IFP SB RAS No. FWGW-2025-0023). In the field of electrophysical research, the work was carried out with the financial support of the Ministry of Science and Higher Education of the Russian Federation (grant No. „FSUS-2024-0020“).

Acknowledgments

The authors are grateful to I.P. Prosvirin (Boreskov Institute of Catalysis of SB RAS) for measuring the elemental composition of samples using the XPS method, and D.V. Marin (NSU) for his help in measuring spectral ellipsometry. The authors would like to thank the VTAN NSU Common Use Center for carrying out measurements on scientific equipment of the Common Use Center.

Conflict of interest

The authors declare that they have no conflict of interest.

References

[1] L. Chua. IEEE Trans. Circuit Theory, **18**, 507 (1971).
[2] D.B. Strukov, G.S. Snider, D.R. Stewart, R.S. Williams. Nature, **453**, 80 (2008).
[3] Panasonic Starts World's First Mass Production of ReRAM Mounted Microcomputers, https://news.panasonic.com/global/press/en130730-2 (2013).
[4] V.A. Volodin, G.N. Kamaev, V.A. Gritsenko, A.A. Gismatulin, A. Chin, M. Vergnat. Appl. Phys. Lett., **114** (3), 033503 (2019).
[5] A.A. Gismatulin, V.N. Kruchinin, V.A. Gritsenko, I.P. Prosvirin, T.-J. Yen, A. Chin. Appl. Phys. Lett., **114**, 233104 (2019).
[6] F. Zhang, V.A. Volodin, E.A. Baranov, V.O. Konstantinov, V.G. Shchukin, A.O. Zamchiy, M. Vergnat. Vacuum, **197**, 110796 (2022).
[7] F. Gul. Ceram. Int., **44**, 11417 (2018).
[8] T.D. Dongale, K.P. Patil, P.K. Gaikwad, R.K. Kamat. Mater. Sci. Semicond. Process., **38**, 228 (2015).
[9] I.D. Yushkov, A.A. Gismatulin, I.P. Prosvirin, G.N. Kamaev, D.V. Marin, M. Vergnat, V.A. Volodin. Appl. Phys. Lett., **125**, 242901 (2024).
[10] A.A. Gismatulin, V.N. Kruchinin, V.A. Gritsenko, I.P. Prosvirin, T.-J. Yen, A. Chin. Appl. Phys. Lett., **114**, 033503 (2019).
[11] M. Ardyanian, H. Rinnert, X. Devaux, M. Vergnat. Appl. Phys. Lett., **89**, 011902 (2006).
[12] F. Zhang, V.A. Volodin, K.N. Astankova, P.V. Shvets, A.Y. Goikhman, M. Vergnat. J. Non-Cryst. Solids, **631**, 122929 (2024).
[13] J.H. Scofield. J. Electron Spectroscopy Relat. Phenomena, **8**, 129 (1976).
[14] D.A. Jishiashvili, E.R. Kutelia. Phys. Status Solidi B, **143**, K147 (1987)
[15] E.L. Murphy, R.H. Good. Phys. Rev., **102**, 1464 (1956).
[16] K.L. Jensen. J. Appl. Phys., **102**, 024911 (2007).
[17] A.A. Gismatulin, V.A. Gritsenko, T.-J. Yen, A. Chin. Appl. Phys. Lett., **115**, 253502 (2019).
[18] G.G. Roberts, J.I. Polanco. Phys. Status Solidi A, **1**, 409 (1970).
[19] V.A. Gritsenko, E.E. Meerson, Y.N. Morokov. Phys. Rev. B, **57**, R2081 (1998).
[20] Ya.I. Frenkel'. *K teorii elektricheskogo proboya v dielektrikah i elektronnyh poluprovodnikah* (B. m., B. i., 1938) t. 8, vyp. 12, p. 1292. (in Russian).
[21] J. Frenkel. Phys. Rev., **54**, 647 (1938).
[22] R.M. Hill. Phil. Mag., **23**, 59 (1971).
[23] H. Adachi, Y. Shibata, S. Ono. J. Phys. D: Appl. Phys., **4**, 988 (1971).
[24] B.I. Shklovsky, A.L. Efros. UFN, **117**, 401 (1975). (in Russian).
[25] B.I. Shklovskiy. Sov. Phys. Semicond., **13**, 53 (1979).
[26] S. Makram-Ebeid, M. Lannoo. Phys. Rev. B, **25**, 6406 (1982).
[27] K.A. Nasyrov, V.A. Gritsenko. J. Appl. Phys., **109**, 093705 (2011).
[28] N.F. Mott, R.W. Gurney. *Electronic processes in ionic crystals* (Oxford, The Clarendon Press, 1940) v. 2, p. 12.
[29] M.A. Lampert. Phys. Rev., **103**, 1648 (1956).
[30] Lampert, Murray A., Peter Mark. *Current injection in solids* (Academic Press, N.Y., 1970).
[31] B. Brar, G.D. Wilk, A.C. Seabaugh. Appl. Phys. Lett., **69**, 2728 (1996).
[32] G. Hautier, A. Miglio, D. Waroquiers, G.-M. Rignanese, X. Gonze. Chem. Mater., **26**, 5447 (2014).
[33] A.A. Gismatulin, G.N. Kamaev, V.A. Volodin, V.A. Gritsenko. Electronics (Basel), **12**, 598 (2023).
[34] N. Vasileiadis, P. Karakolis, P. Mandylas, V. Ioannou-Sougleridis, P. Normand, M. Perego, P. Komninou, V. Ntinas, I.-A. Fyrigos, I. Karafyllidis. IEEE Trans. Nanotechnol., **20**, 356 (2021).
[35] T.V. Perevalov, V.A. Volodin, G.N. Kamaev, G.K. Krivyakin, V.A. Gritsenko, I.P. Prosvirin. J. Non-Cryst. Solids., **529**, 119796 (2020).
[36] S.D. Nehate, A. Prakash, P.D. Mani, K.B. Sundaram. ECS J. Solid State Sci. Technol., **7**, 87 (2018).
[37] V.A. Gritsenko, V.A. Volodin, T.V. Perevalov, V.N. Kruchinin, A.K. Gerasimova, V.S. Aliev, I.P. Prosvirin. Nanotechnology, **29**, 425202 (2018).
[38] D.R. Islamov, V.A. Gritsenko, C.H. Cheng, A. Chin. Appl. Phys. Lett., **103**, 232904 (2013).

Translated by A.Akhtyamov